Journal of Materials Science & Technology 161 (2023) 170–179

Contents lists available at ScienceDirect

Journal of Materials Science & Technology

journal homepage: www.elsevier.com/locate/jmst

Review Article

Magnesium borohydride $Mg(BH_4)_2$ for energy applications: A review

Xiao Li[a], Yigang Yan[b], Torben R. Jensen[c], Yaroslav Filinchuk[d,*], Iurii Dovgaliuk[e], Dmitry Chernyshov[f], Liqing He[a], Yongtao Li[g], Hai-Wen Li[a,*]

[a] Hefei General Machinery Research Institute, Hefei 230031, China
[b] Institute of New Energy and Low-Carbon Technology, Sichuan University, Chengdu 610207, China
[c] Department of Chemistry and Interdisciplinary Nanoscience Center, Aarhus University, Langelandsgade 140, Aarhus C 8000, Denmark
[d] Institute of Condensed Matter and Nanosciences, Université Catholique de Louvain, Place L. Pasteur 1, B-1348, Louvain-la-Neuve, Belgium
[e] Institut des Matériaux Poreux de Paris, UMR 8004 CNRS, Ecole Normale Supérieure, Ecole Supérieure de Physique et de Chimie Industrielles de Paris, PSL Université, Paris 75005, France
[f] Swiss-Norwegian Beamlines at the European Synchrotron Radiation Facility, 71 Avenue des Martyrs, Grenoble 38000, France
[g] School of Materials Science and Engineering, Anhui University of Technology, Maanshan 243002, China

ARTICLE INFO

Article history:
Received 30 December 2022
Revised 27 February 2023
Accepted 14 March 2023
Available online 7 May 2023

Keywords:
Hydride
Hydrogen storage
Gas adsorption
Hydrogen adsorption
Electrolyte

ABSTRACT

$Mg(BH_4)_2$ with several polymorphs, known as a high capacity (14.9 wt.%) hydrogen storage material, has become more intriguing due to the recently found new functions of gas physisorption and ionic conductivity. Here we review the state-of-the-art on the energy related functions of $Mg(BH_4)_2$. $Mg(BH_4)_2$ tends to form the stable intermediate $[B_{12}H_{12}]^{2-}$ when the dehydrogenation temperature is above 400 °C, the strong B-B bonding of which makes the rehydrogenation condition very harsh. In contrast, lower borane intermediate $[B_3H_8]^{2-}$ facilitates the rehydrogenation even at a mild condition of 100 °C, suggesting the possibility of reversible hydrogen storage in $Mg(BH_4)_2$. The porous polymorph γ-$Mg(BH_4)_2$ shows attractive gas adsorption properties in view of its unique hydridic surface and pore shape, and potentially can be applied in hydrogen adsorption and Kr/Xe selectivity. A new diffraction-based adsorption methodology was developed to characterize adsorption thermodynamics and kinetics of γ-$Mg(BH_4)_2$, providing a novel idea for the characterization of crystalline porous materials. Moreover, the potential of $Mg(BH_4)_2$ as an electrolyte is discussed in the last part. $Mg(BH_4)_2$·THF/DME acts as a liquid electrolyte in Mg-batteries, while anion substituted or neutral molecule derivatives of $Mg(BH_4)_2$ can act as solid-state electrolyte.

1. Introduction

The over-reliance on fossil fuels in the past decades has caused alarming environmental problems such as climate change and global warming. Exploitation of renewable and clean energy, e.g. wind, solar, tide, etc. to replace fossil fuels is of utmost importance to reduce carbon emissions and develop a sustainable energy system. Due to the intermittent nature of renewable energy resources, the development of efficient energy storage techniques is essential to realize a wider application. Renewable electricity can be stored directly in a battery or be used for electrolysis of water to produce oxygen and hydrogen [1]. Hydrogen has the highest energy density of all known substances, 120.0 MJ/kg H_2 (lower heating value), which is a factor × 3 higher than that of gasoline. On the other hand, hydrogen is the lightest element ($Z = 1$), and it is a low-density gas with $\rho(H_2(g)) = 0.0899$ g/L at 20 °C and 1 bar, which is only 7% of the density of atmospheric air. The density can be increased to 40 g/L when pressure is compressed up to 700 bar. Liquefied hydrogen has a higher density of $\rho(H_2(l)) = 70.8$ g/L at -253 °C [2]. Compressed and liquefied hydrogen are both feasible ways for hydrogen storage, which can contribute to the large-scale and long-term energy storage [3,4].

Hydrogen can also be stored in the solid state hydrides, e.g. metal hydrides [5–9] and complex hydrides [10–12]. Among them, metal borohydrides have expanded significantly during the past decades [13–21]. Among these compounds, magnesium tetrahydridoborate, also known as magnesium borohydride, $Mg(BH_4)_2$, was found. This compound is very unique regarding polymorphism, chemical and physical properties which are highlighted in these reviews [22,23]. Magnesium borohydride both exists as crystalline polymorphs [24–28] with nano-porous MOF-like structures but also a very dense polymorph with extreme volumetric hydrogen density, ρ_V ~146 kg/m^3 and also high gravimetric hydrogen capacity of, ρ_m ~14.9 wt.% [26,28], which by far exceeds the tar-

* Corresponding authors.
E-mail addresses: yaroslav.filinchuk@uclouvain.be (Y. Filinchuk), lihaiwen66@hotmail.com (H.-W. Li).

https://doi.org/10.1016/j.jmst.2023.03.040
1005-0302/

get for onboard hydrogen storage announced by Department of Energy of United States (5.5 wt.% and 40 kg/m^3 by 2025) [29]. $Mg(BH_4)_2$ was first synthesized and discovered in 1950 [30]. The early study focused on the physical and chemical properties of this compound and its adducts [31,32]. The hydrogen storage properties of $Mg(BH_4)_2$ were systematically studied from 2007 [33,34] and numbers of research worked on its decomposition mechanism and the improvement of de/re-hydrogenation [11,35–38].

γ-$Mg(BH_4)_2$ has been attracting increasing interest due to its complicated polymorphism for a seemingly simple ionic compound. In 2009, it was noticed that the α-polymorph contains empty pores of the size of water molecules [24]. In 2011, the first example of borohydrides with functional nano-porous scaffold structure was discovered, γ-$Mg(BH_4)_2$, which has about ~33% open space in the structure and therefore shows interesting gas adsorption properties [26]. It contains tubular porous channels which can accommodate small molecules such as N_2, H_2 and dichloromethane (CH_2Cl_2) [26]. N_2 adsorption properties determined the pore size at ~7 Å, in good agreement with the structural information. However, the BET surface area of γ-$Mg(BH_4)_2$ is determined as 246 m^2/g, while the calculated surface area from crystal structure is 1505 m^2/g. The huge disagreement is mainly caused by a presence of an amorphous fraction of $Mg(BH_4)_2$, as well as the larger effective radius of N_2 compared to a small pore in γ-$Mg(BH_4)_2$. Diffraction experiments show the maximum capacity of N_2 per Mg atom is 0.66, i.e. γ-$Mg(BH_4)_2{\cdot}0.66N_2$.

$Mg(BH_4)_2$ also has the potential as an electrolyte in battery systems. In 2012, $Mg(BH_4)_2$ was found to have potential as an electrolyte in a novel type of magnesium batteries, when dissolved in an organic liquid [39]. However, liquid organic electrolytes are of significant safety concerns, and could be avoided using a solid inorganic electrolyte. That would provide a novel all-solid-state battery. The challenge is that cations typically have little mobility in the solid state, e.g. magnesium borohydride has negligible cationic conductivity, $\sigma(Mg^{2+})$ ~10^{-12} S cm^{-1} [40], and also electronic conductivity, σ_e ~10^{-9} S cm^{-1}. Thus, this material behaves as an insulator. Surprisingly, when magnesium in $Mg(BH_4)_2$ is coordinated to a neutral molecule, the Mg^{2+} conductivity may be increased by several orders of magnitude [41,42]. During the past few years, a series of novel compounds, $Mg(BH_4)_2{\cdot}R$, where magnesium is complexed with a neutral molecule, such as ammonia (NH_3), ethylenediamine ($H_2NCH_2CH_2NH_2$), tetrahydrofuran (C_2H_4O), etc. have been obtained. These compounds have high cationic (Mg^{2+}) conductivity also at moderate temperatures and thus are fundamental for the design of new solid state inorganic batteries [43–47]. It is worth mentioning that Mg-ion battery is more resource abundant than Li-ion battery, which makes it potential to be an excellent candidate in the batteries field.

This review will focus on $Mg(BH_4)_2$ and its synthesis methods, polymorphism and phase transition, as well as the main properties including hydrogen storage, gas adsorption and ionic conductivity will be overviewed systematically. As the hydrogen storage properties of $Mg(BH_4)_2$ have been summarized in the recent reviews [22,23,48], we will put more emphasis on the latter two research directions. The summary of the main functions of $Mg(BH_4)_2$ is shown in Fig. 1 [26,34,39,49–51].

2. Synthesis and structure

2.1. Synthesis methods of $Mg(BH_4)_2$

The synthesis of $Mg(BH_4)_2$ was first proposed by Wiberg and Bauer [30] in 1950. They found that the magnesium diethyl and diborane (B_2H_6) could slowly react at room temperature according to the following reaction:

$$3MgR_2 + B_2H_6 \rightarrow 3MgH_2 + 2BR_3 \quad (1)$$

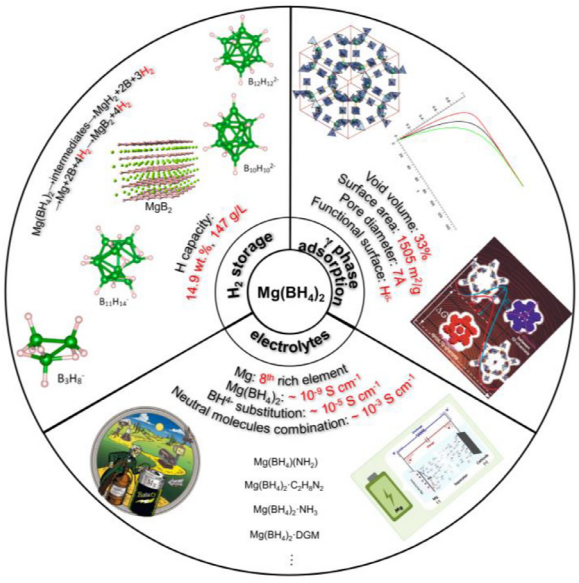

Fig. 1. Functions of magnesium borohydride as an electrolyte in novel types of magnesium batteries, for solid state hydrogen storage or for gas storage [26,34,39,49–51].

$$3M_gH_2 + 3B_2H_6 \rightarrow 3M_g(BH_4)_2 \quad (2)$$

However, the high toxicity and flammability of diborane and of its derivatives make this method not applicable. Later two synthesis strategies have been developed: solvent-based synthesis and solvent-free synthesis (solid phase synthesis). Typical synthesis methods reported in the past years are summarized in Table 1.

2.2. Polymorphism of $Mg(BH_4)_2$ and phase transition

One of the most interesting properties of $Mg(BH_4)_2$ is its polymorphism and the related phase transitions. $Mg(BH_4)_2$ shows the most complex crystalline phases among all the metal borohydrides [67]. A number of studies reveal the following polymorphs (meta)stable at ambient conditions: the hexagonal ($P6_122$) α−phase [24], orthorhombic (*Fddd*) β-phase and its closely related β'-phase [25], the porous cubic (*Ia*-3*d*) γ-phase [26], the dense high-pressure tetragonal ($P4_2nm$) δ-phase [26], that was later revised in a $I4_1/acd$ superstructure with a more complex order of the BH_4 groups. The latter is obtained at high pressures but is quenchable to ambient conditions. Besides that a trigonal ($P3_112$) ζ-phase [27], isostructural to $Mn(BH_4)_2$ [68], is observed in a narrow temperature range, along with so-called ε phase. Furthermore, the amorphous $Mg(BH_4)_2$ also forms both during synthesis and via pressure-induced collapse of the porous γ-phase [28]. Remarkably, the high-pressure phase undergoes a transition back to the porous phase upon heating. It is likely a polymorphism occurs for magnesium borohydride, namely structurally different amorphous phases forming, for example during the thermal treatment of the γ-phase and after its pressure-induced collapse. The summary of structural parameters of $Mg(BH_4)_2$ can be found in Table 2, as well as in Refs [22,23]. Some phases can be directly synthesized by solvent-based methods while some phases can be observed after a phase transition [67]. The condition of phase transition is summarized in Fig. 2 [16,24–27,33,69–74].

A large number of $Mg(BH_4)_2$ polymorphs and their (meta)stability in a wide *p*-*T* range suggest that the structural reorganization is linked to breaking significant barriers related to Mg-BH_4 bonding. This interaction is not seen as entirely ionic, but more like a bonding between metal and ligand in the MOFs

Table 1
Summary of synthesis routes of $Mg(BH_4)_2$ using solvent-based methods or solvent-free methods.

Methods	Reaction pathway	Condition/comment	Refs.
Solvent-based	$2NaBH_4+MgCl_2\rightarrow Mg(BH_4)_2+2NaCl$	Cold ethanol/diglyme.	[52,53]
	$MgH_2+2(C_2H_5)_3N{\cdot}BH_3\rightarrow Mg(BH_4)_2{\cdot}2(C_2H_5)_3N$	100 °C under argon; vacuum + 100–170 °C to remove adduct.	[54]
	$MgH_2+B_2H_6\rightarrow Mg(BH_4)_2$	In ether; vacuum + 150–180 °C to remove ether.	[55,56]
	$MgX_2+MBH_4\rightarrow Mg(BH_4)_2+MX$; M=Na, Li; X=Cl, Br	Ball milling in diethyl ether; vacuum + high T to remove diethyl ether.	[33,57,58]
	$3Mg(C_4H_9)_2+8BH_3{\cdot}DMS\rightarrow 3Mg(BH_4)_2{\cdot}2DMS+2B(C_4H_9)_3{\cdot}DMS$	In toluene, excess $BH_3{\cdot}S(CH_3)_2$, vacuum + high T to remove DMS.	[59]
Solvent-free	$Mg+2B+4H_2\rightarrow Mg(BH_4)_2$	Ball milling, high p and T, low yield, hardly can obtain $Mg(BH_4)_2$	[60]
	$MgCl_2+2MBH_4\rightarrow Mg(BH_4)_2+2MCl$, M=Li, Na	Ball milling under N_2, need further purification	[61]
	$MgB_2+4H_2\rightarrow Mg(BH_4)_2$	Pre-milled MgB_2, high T=400 °C, long time 108 h	[62–66]

Table 2
Polymorphs of $Mg(BH_4)_2$ observed by experiments.

Phase	Space group	Cell parameters (Å)	Cell volume (Å^3)	Refs.
α-$Mg(BH_4)_2$	$P6_122$	a=b=10.33555 c=37.08910 α=β=90° γ=120°	3431.21	[24]
β-$Mg(BH_4)_2$	$Fddd$	a=37.04892 b=18.49186 c=10.85945 α=β=γ=90°	7439.82	[25]
γ-$Mg(BH_4)_2$	Ia-$3d$	a=b=c=15.7575 α=β=γ=90°	3912.57	[26]
δ-$Mg(BH_4)_2$	$P4_2nm$ ($I4_1/acd$)	a=b=5.4361 c=6.1468 α=β=γ=90°	181.65	[26]
$\zeta(\varepsilon)$-$Mg(BH_4)_2$	$P3_112$	a=b=10.424 c=10.729 α=β=90° γ=120°	1009.7	[27]

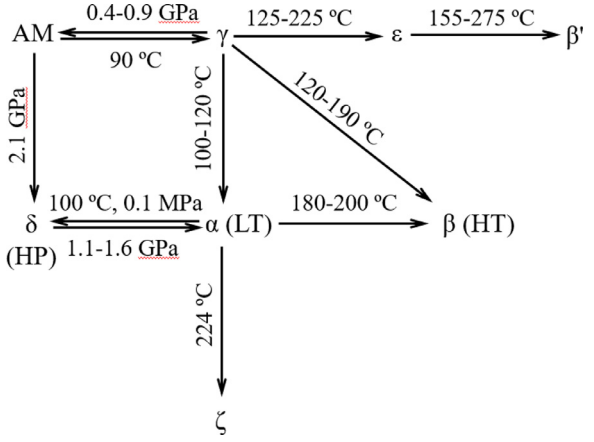

Fig. 2. Illustration of phase transition of $Mg(BH_4)_2$. AM = amorphous phase, LT = low-temperature phase, HT = high-temperature phase, HP = high-pressure phase.

family [26]. As a consequence, we can consider $Mg(BH_4)_2$ polymorphs as different topologies of linking nodes by borohydride linkers. Indeed, in all known $Mg(BH_4)_2$ structures, Mg atom has a tetrahedral coordination by four BH_4 groups, moreover often with only one specific MgH_8 coordination known as snub disphenoid, while the BH_4 group is always linearly coordinated by two Mg, via it opposite tetrahedral edges. With such a fixed local geometry of the constituents, only the topology of the framework varies. Several crystal structures of $Mg(BH_4)_2$ polymorphs are shown in Fig. 3, presented for simplicity as ionic structures assembled by packing cations and anions [75].

3. Hydrogen storage properties

$Mg(BH_4)_2$ possesses high hydrogen capacity both gravimetric (14.9 wt.%) and volumetric (145–147 g/L, high-pressure δ-phase). However, the practical applications of $Mg(BH_4)_2$ are currently restricted by two factors. First, the de/hydrogenation conditions are very harsh. The dehydrogenation route of $Mg(BH_4)_2$ has been proved to be a very complicated process [71,76–80]. It starts at approximately 250 °C and the dehydrogenation upon heating is accompanied by the formation of intermediate borates with chemical formula $B_xH_y^{n-}$, including $[B_3H_8]^-$, $[B_5H_9]^-$, $[B_{10}H_{10}]^{2-}$, $[B_{11}H_{14}]^-$, and $[B_{12}H_{12}]^{2-}$, etc. The $B_xH_y^{n-}$ tends to grow up to larger boranes with elevated temperature and it tends to form stable $[B_{12}H_{12}]^{2-}$ when the dehydrogenation temperature is above 400 °C [50,71,81–87]. There may be large divergences between theoretical calculations and experimental amounts of desorbed hydrogen, as long as impurities form due to the formation of different intermediates. The latest study [67] indicates that factors, such as synthesis route, residual impurities, starting crystalline phase, etc. also influence the phase transition and thermal decomposition of $Mg(BH_4)_2$. Theoretically, the enthalpy change from $Mg(BH_4)_2$ to MgB_2 only requires about 30–50 kJ/mol, indicating the dehydrogenation tem-

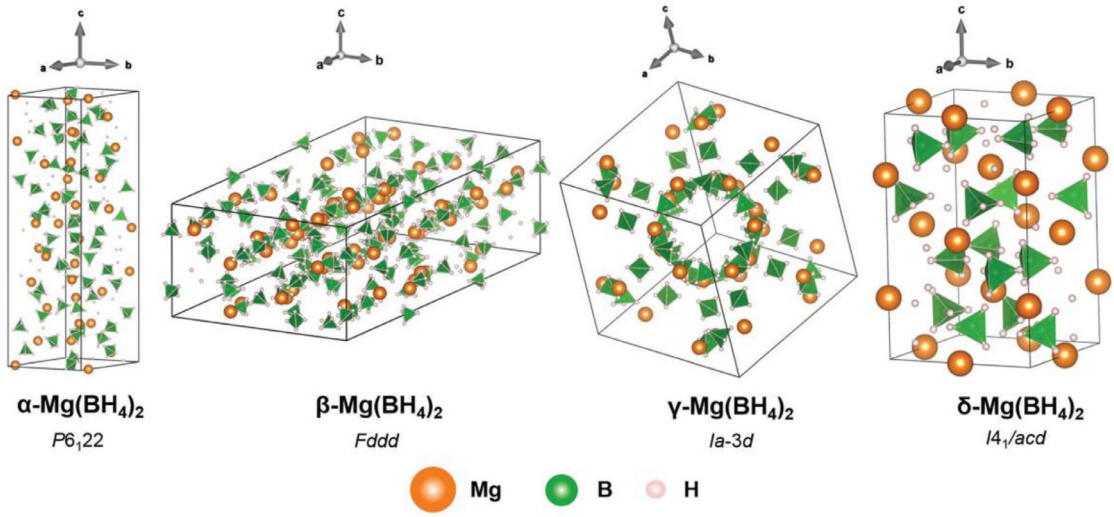

Fig. 3. Reported crystal structures of different polymorphs of $Mg(BH_4)_2$. Mg atoms are shown as orange spheres, BH_4 groups as green tetrahedra, and unit cells are defined by black lines [75].

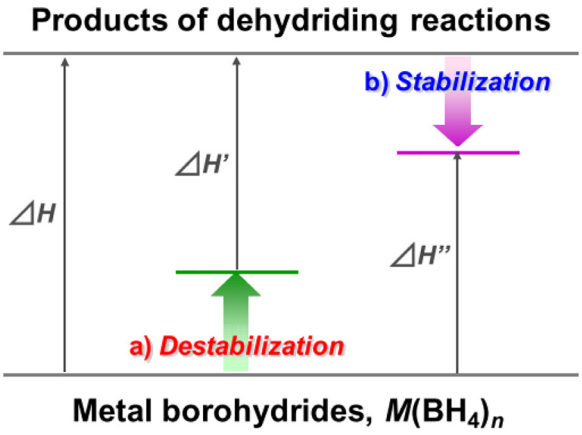

Fig. 4. Schematic illustration of how to reduce dehydrogenation enthalpy change of metal borohydrides [94].

perature is near room temperature, whereas the actual desorption occurs between 250 and 580 °C due to the high dehydrogenation energy barrier [25,88]. The second factor is its poor reversibility and cyclability of de/hydrogenation, which largely depends on the dehydrogenation products [37,89]. Lower borane $[B_3H_8]^-$ formed at a moderate dehydrogenation condition of 200 °C was found to facilitate the rehydrogenation, which starts at ~100 °C and yields ~22 wt.% of $[BH_4]^-$ along with the formation of (closo-hydro)borates and volatile boranes [90,91]. On the other hand, higher borane $[B_{12}H_{12}]^{2-}$ can also be rehydrogenated back to $[BH_4]^-$, whereas it requires a severe condition of above ~400 °C and 40 MPa hydrogen pressure [92,93].

Extensive studies have been carried out to improve the hydrogen storage properties of $Mg(BH_4)_2$, via thermodynamic tailoring and kinetic promoting. In terms of thermodynamics, the enthalpy change of dehydrogenation of $Mg(BH_4)_2$ (ΔH_{deh}) has a great impact on its dehydrogenation temperature. Li et al. [94] pointed out that the ΔH_{deh} can be reduced through two approaches: destabilization of metal borohydrides and stabilization of dehydrogenation products, as shown in Fig. 4. The objective of destabilization can be achieved by producing multi-metallic cation borohydrides and/or building composites with hydrides, alanates, amides and so on. According to theoretical predictions, the ΔH_{deh} has a strong correlation with Pauling electronegativity of the metal cation in borohydrides [95], so the dehydrogenation temperature can be tuned by adjusting the type and ratio of metal cations, such as Li-Mg, Na-Mg, K-Mg, and Ca-Mg borohydride systems [96–103]. The composites obtained by adding binary hydrides (e.g., AlH_3, CaH_2, NaH, LiH [104,105]), alanates (e.g., $LiAlH_4$, $NaAlH_4$ [106–108]), amides (e.g., $LiNH_2$, N_2H_4, NH_3 [109–112]), etc. are effective ways to change the dehydrogenation pathway and so that to improve the thermodynamic properties [113].

Doping and nanoconfinement are two approaches for kinetic improvement. Doping with additives is an effective way to improve the dehydrogenation kinetics of $Mg(BH_4)_2$. The additives can be classified into metals [34,114–116], metal oxides [72,89,117,118], metal halides [119–125], and carbon-based materials (carbon nanotubes, graphene, MXene, etc.) [80,126–131]. High-energy ball milling is usually applied to obtain $Mg(BH_4)_2$-additive systems with homogeneous mixture. The additives tend to react with $Mg(BH_4)_2$ during the milling or heating process to generate the catalytic species, while the exact catalytic mechanism is still under investigation [48]. Nanoconfinement can reduce the diffusion distance, increase the grain boundaries and introduce more defects on the surface, promoting kinetic properties [132]. Nanoconfined materials can be obtained by wet impregnation, melt infiltration, *in-situ* synthesis and confinement in nanoporous materials [133–141]. Detailed information on the state of the art on improving de/re-hydrogenation properties of $Mg(BH_4)_2$ is expected to refer to recent reviews [22,23,48].

4. Studies of adsorption by γ-$Mg(BH_4)_2$

Since $Mg(BH_4)_2$ has high hydrogen capacity, most studies have only focused on the improvement of its hydrogen storage performance. However, γ-$Mg(BH_4)_2$ shows a unique porous structure among all the other polymorphs. It is also the first example of a porous framework with the surface made entirely of hydridic atoms. It contains a tubular-shaped pore channel with about 7 Å in diameter, and the narrowest part of the pore channel (the aperture) is defined by two hydrogens from the BH_4 groups, which is about 5.8 Å (the crystal structure and pore size/shape of γ-$Mg(BH_4)_2$ is shown in Fig. 5). The unique hydridic surface [118,142] gives a chance to discover some unusual adsorption behavior. A few studies [26,49,143–145] explored the adsorption properties of different gases, such as N_2, H_2, C_2H_6, Ar, Kr and Xe, both from experimental and theoretical point of view.

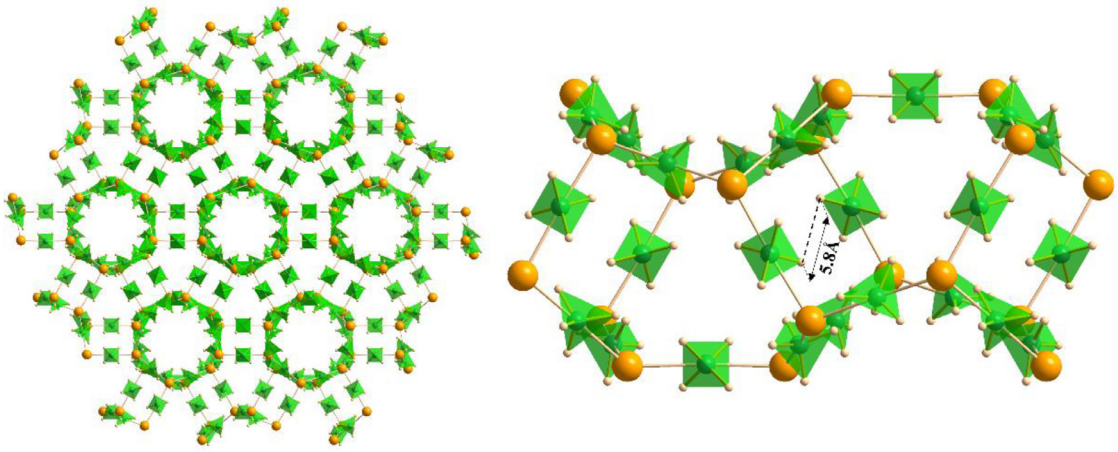

Fig. 5. The 2 × 2 × 2 unit cell structure of γ-$Mg(BH_4)_2$ viewed from [109] (left) and pore size/shape viewed from [−111] (right). Mg atoms are shown as orange sphere, B atoms as dark green sphere, and H atoms as tan sphere. The BH_4 anion is shown as light green tetrahedra.

A new methodology that is based on diffraction methods was developed to characterize adsorption in γ-$Mg(BH_4)_2$, both from the point of view of structural study, but also aiming to access the macroscopic properties. The *in-situ* diffraction data are collected under various gas pressures at fixed temperatures (isotherms), temperature ramp at fixed pressures(isobars) or as a function of time (adsorption kinetics). Afterwards, the position and orientation of guest molecules are first obtained by a structure solution algorithm, e.g. global optimization in direct space, followed by a sequential Rietveld refinement of this model along the adsorption isotherms, isobars and/or kinetics. Information about individual guest's atomic positions and occupancies can be obtained, thus giving access to equilibrium pressure-temperature-composition diagrams and cooperative interactions.

4.1. Adsorption thermodynamics and kinetics study

The initial work on adsorption of N_2 and H_2 in γ-$Mg(BH_4)_2$ was done in 2011 [26], using 3 isobars of nitrogen sorption, as well as 2 isobars for hydrogen adsorption; the interaction of both gasses was characterized by synchrotron X-ray powder diffraction. Nitrogen molecules were found disordered in the centres of the pores, with the maximum capacity of 1 N_2 molecule per pore (equivalent to 2/3 N_2 per Mg atom). Adsorption isobars were obtained at 0.34, 3.45 and 30.6 bar, resembling the sigmoidal function, and thus were fitted by the Logistic function. Clausius-Clapeyron equation was used to estimate the isosteric heat of nitrogen adsorption, which turned out to be nearly constant with loading, at the average value of 14.7 kJ/mol. Since the hydrogen molecule is a weak scatterer of X-rays, it was assumed that H_2 molecules take the same position as N_2. However, a simulation study [145] (introduction to this study is in Section 4.2) predicted the capacity of H_2 molecule in γ-$Mg(BH_4)_2$ is 0.9 H_2 per Mg, which is beyond the capacity of N_2, indicating the two gases take different positions. Therefore, further investigation of H_2 adsorption in γ-$Mg(BH_4)_2$ should be done by neutron diffraction to accurately detect the adsorption site of H_2.

Dovgaliuk et al. [49,143,144] studied the adsorption thermodynamics and kinetics of γ-$Mg(BH_4)_2$ serially from 2017 to 2021. Firstly, they studied N_2 and C_2H_6 adsorption isobars by γ-Mg(BH4)$_2$ from *in-situ* X-ray powder diffraction experiments [143] and derived a thermodynamic description, based on Gorsky-Bragg-Williams mean-field approach for the lattice-gas Ising model, allowing to determine the thermodynamic parameters such as enthalpy, entropy and adsorption cooperativity from an isobar. The expression used is the following:

$$T = \frac{\Delta H_i - \Gamma_i(1-2\gamma_i)}{\Delta S_i - R\ln\left(\frac{1-\gamma_i}{\gamma_i}\right)} \quad (3)$$

The subscript i is associated with guest adsorption by the site I, Γ is cooperativity, and γ is a fraction of the adsorbed guest molecules. Furthermore, the parameter Γ, which is a general measure of guest-guest interactions, accounts for the cooperative interactions for the guest molecules occupying different pores, those indirect interactions are mediated by elastic perturbations induced by guest molecules in the flexible framework structures.

Later, adsorption of larger molecules such as Kr by γ-$Mg(BH_4)_2$ was studied in a form of quasi-equilibrium and non-equilibrium adsorption isobars. This enabled to estimate kinetic parameters (such as an activation energy) by analyzing the kinetic hysteresis [144]. This work exhibits a transition from the study of thermodynamics using equilibrium isotherms and isobars, towards non-equilibrium kinetics that may influence these data to the point the kinetic hysteresis appears. This opens a door to estimating the activation barriers.

A more ingenious approach was proposed afterwards to precisely study the adsorption kinetics of Ar, Kr and Xe in γ-$Mg(BH_4)_2$ [49]. Time dependent *in-situ* diffraction at fixed *p-T* condition was used to measure ten thousand of powder diffraction patterns with a high time resolution. After analyzing the data by sequential Rietveld refinement and refining guest occupancies, the diffusion barriers (activation energy) for three noble gases can be extracted by applying Arrhenius equation. The medium-sized Kr shows two activation barriers attributed to two diffusion pathways, one along the pore channel and the other between the channels, while the smaller and larger Ar and Xe only show one diffusion barrier (results shown in Fig. 6 [49]). This phenomenon indicates a potential application of γ-$Mg(BH_4)_2$ for selective adsorption of Kr and Xe.

4.2. Hydrogen adsorption in γ-$Mg(BH_4)_2$

Besides the first (experimental) study of H_2 adsorption in γ-$Mg(BH_4)_2$ [26], another work has been reported on the adsorption behavior of hydrogen in γ-$Mg(BH_4)_2$ from theoretical point of view. The authors [145] used the grand canonical Monte Carlo (GCMC) method to simulate the hydrogen adsorption in γ-$Mg(BH_4)_2$ in ZIF-72 of the same topology, followed by fitting the isotherms with Langmuir, quadratic and line functions for different pressure steps. γ-$Mg(BH_4)_2$ was predicted to adsorb 3.44 wt.% H_2 at 78 K, at around 30 bar, corresponding to γ-$Mg(BH_4)_2{\cdot}0.9H_2$.

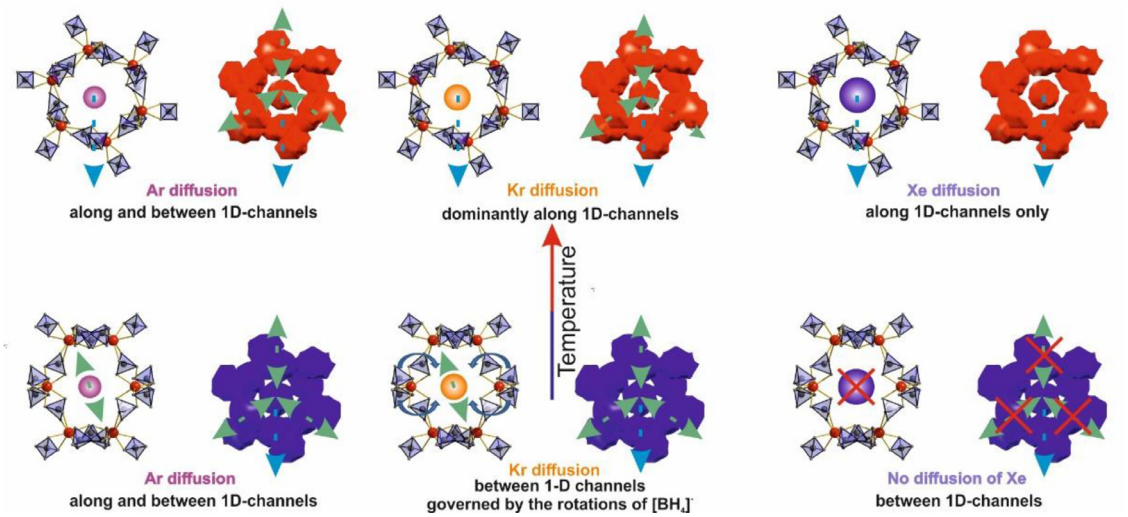

Fig. 6. Illustration of the diffusion pathways of Ar, Kr and Xe in γ-$Mg(BH_4)_2$ [49].

As a result, the total hydrogen capacity of γ-$Mg(BH_4)_2$ can finally reach 18.34 wt.% when considering both chemical bond storage and physisorption storage.

4.3. Prospects for adsorption of other gases

In the above study, γ-$Mg(BH_4)_2$ shows interesting host-guest interaction which is due to its unique surface characteristics decorated by hydridic hydrogen. Adsorption of other gases, such as small-size noble gases (He, Ne, Ar), methane and other flammable alkanes/olefins, could be predicted to show unexpected behaviors, potentially to be applied in gas storage and separation.

Compared to classical volumetric and gravimetric gas adsorption measurements, diffraction-based method, which is mentioned at the beginning of this section, exhibits two more advantages besides being able to simultaneously observe the gas adsorption behavior both macro- and microscopically. First, it is only sensitive to crystalline phases and one can focus on the specific crystalline phase which needs to be addressed. There is a fraction of dense amorphous phase of $Mg(BH_4)_2$ variable from one batch to another [49,146], which influences systematically the gas uptake measured by volumetric or gravimetric methods. Secondly, diffraction-based methods can access adsorption isobars, which are hardly obtainable by volumetric methods, as the non-isothermal calibration is overwhelmingly complicated. Wider temperature range is more informative since it contains a wider range of chemical potential, thus better suited for intuitively displaying specific features of guest-host and guest-guest interactions.

5. Applications in batteries

Magnesium batteries are considered potential future alternatives to the currently commercialized Li-ion battery for multiple reasons: (i) much larger and more evenly distributed abundance of magnesium resources in the crust of the earth, i.e. ~2.7 wt.% compared to 0.0065 wt.% of Li, but also 0.1 wt.% of all seawater is magnesium. (ii) Magnesium metal has high theoretical gravimetric and volumetric capacities of 2200 mAh g^{-1} and 3835 mAh cm^{-3}, and the latter is about double that of Li (i.e. 2036 mAh cm^{-3}). (iii) Magnesium also has a low standard reduction potential of -2.4 V versus the standard hydrogen electrode (SHE) along with lower tendency to grow as dendrite type crystals during charge and discharge of the battery. The current lithium-ion battery technology is very successful but appears to be fully developed with only very limited potential for further improvement of energy capacity and performance. Moreover, there is a significant safety issue related to the use of a liquid-organic electrolyte. This has called for alternatives chemistries, such as magnesium-based batteries, and new technologies, such as inorganic solid-state batteries. Solid-state batteries (SSB) have several advantages over the present liquid-state Li-ion batteries, e.g. (i) potentially higher energy density, (ii) improved safety and lifetime, due to removal of the flammable and unstable liquid electrolyte; (iii) possible operation in a larger temperature range since organic polymeric electrolytes may crystallize upon cooling (e.g. at $T < 0$ °C) or decompose upon heating (e.g. at $T > 80$ °C). However, a fundamental drawback is to achieve fast divalent cationic, e.g. Mg^{2+}, migration in liquid or solid state, since such cations have larger charge-density and interact stronger with the surrounding coordination sphere [147]. In the following, we discuss the fact that magnesium borohydride has been the basis for game-changing discoveries both within novel liquid electrolytes and solid state electrolytes.

5.1. Liquid electrolytes for magnesium batteries

In 2012, Mohtadi et al. [39] reported the solvation of $Mg(BH_4)_2$ in THF or DME as electrolyte for reversible Mg deposition/dissolution. By mixing with $LiBH_4$, the ionic conductivity of $Mg(BH_4)_2$ ether solution can be improved and Coulombic efficiency (CE) increases proportionally to the mass ratio of $LiBH_4/Mg(BH_4)_2$. A prototype Mg battery with a Chevrel phase Mo_6S_8 cathode, an Mg metal anode, and $LiBH_4/Mg(BH_4)_2$ DME solution was demonstrated at 128.8 mA g^{-1}. The value of CE can be further improved by replacing the ether solvent with diglyme [148]. However, $Mg(BH_4)_2$-based etheral solutions have low anodic stability of 1.7 V *vs.* Mg/Mg^{2+} and low chemical stability in the presence of water. To improve the anodic stability, other more stable *closo*-borate cage-like anions, such as $B_{12}H_{12}^{2-}$ and $CB_{11}H_{12}^{-}$, were used [149]. The $Mg(CB_{11}H_{12})_2$ tetraglyme solution shows an improved stability towards most current collectors with an anodic stability of ≥3.0 V *vs.* Mg/Mg^{2+}.

5.2. Anion substituted magnesium borohydride as solid state electrolyte[

In all polymorphs of magnesium borohydride, $Mg(BH_4)_2$, Mg is coordinated to four BH_4^- complexes via edge-sharing, i.e. Mg^{2+} coordinates eight partly negatively charged hydrogen atoms in the

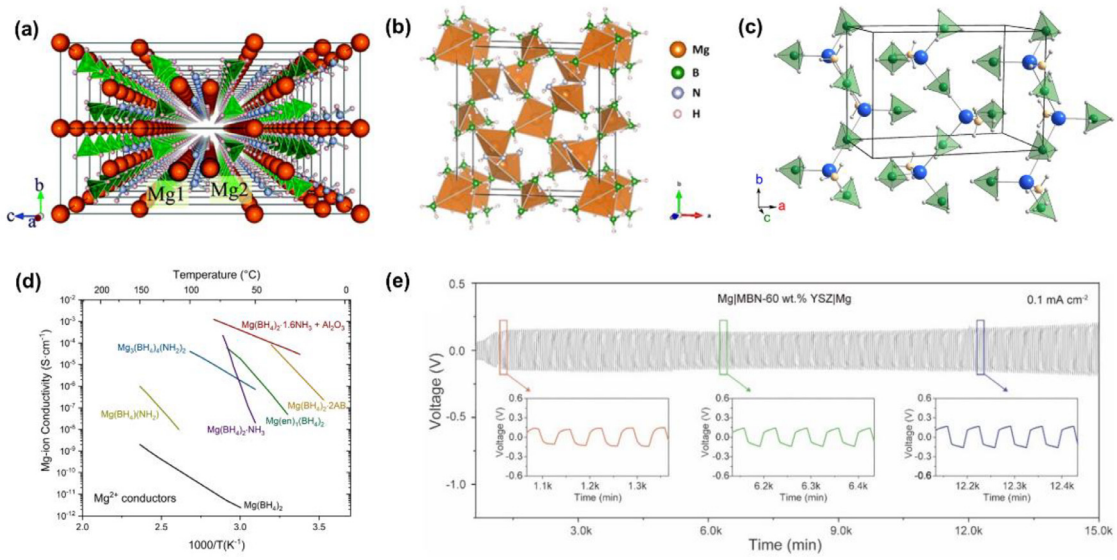

Fig. 7. (a–c) Crystal structure of $Mg(BH_4)(NH_2)$, $Mg_3(BH_4)(NH_2)_2$, and $Mg(BH_4)\cdot NH_3$, (d) Mg^{2+} conductivity plots of typical $Mg(BH_4)_2$-based solid-state electrolytes, (e) long-term cycling of $Mg(BH_4)_2\cdot 1.5NH_3$-60 wt.% YSZ nanocomposite at 0.1 mA cm^{-2} at 60 °C. Abbreviations: en = ethylenediamine, AB = ammonia borane, YSZ = Y_2O_3-stabilized ZrO_2.

first coordination sphere. This polar-covalent-ionic bonding leads to negligible cationic ($\sigma(Mg^{2+})$ ~10^{-12} S cm^{-1} at room temperature) and electronic conductivity of $Mg(BH_4)_2$. Substitution in the BH_4^- anion lattice with other anions such as halides, NH_2^- or AlH_4^-, has been used to tailor structural, chemical and physical properties, and also to enhance cationic conductivity.

Ikeshoji et al. [150] proposed that the Mg^{2+} conduction of $Mg(BH_4)_2$ could be improved by partial replacement of BH_4^- with AlH_4^-, which was supported by theoretical simulation [151]. Higashi et al. [152] reported the Mg^{2+} conductivity of 10^{-6} S cm^{-1} at 150 °C in $Mg(BH_4)(NH_2)$, which allows the reversible Mg stripping/plating. $Mg(BH_4)(NH_2)$ exhibits tunneling structures with a Mg zigzag chain contributing to the Mg migration (Fig. 7(a)). Ruyet et al. [45] improved the Mg^{2+} conductivity of $Mg(BH_4)(NH_2)$ to 3×10^{-6} S cm^{-1} at 100 °C by balling milling and heat treatment, in which the improved conductivity is attributed to the presence of an additional amorphous phase. Ruyet et al. [153] further synthesized the single-phase $Mg_3(BH_4)_4(NH_2)_2$, as shown in Fig. 7(b), with higher thermal stability and a high Mg^{2+} ionic conductivity of 4.1×10^{-5} S cm^{-1} at 100 °C. The reversible Mg deposition/stripping was demonstrated at 100 °C when using $Mg_3(BH_4)_4(NH_2)_2$ as solid electrolyte.

5.3. Neutral molecule derivatives of magnesium borohydride as solid state electrolytes

Another approach is to introduce neutral molecules, such as ethylenediamine (*en*, $NH_2(CH_2)_2NH_2$), NH_3 and NH_3BH_3, to $Mg(BH_4)_2$. Roedern et al. [44] reported the improvement of Mg^{2+} conductivity to 6×10^{-5} S cm^{-1} at 70 °C by the introduction of one molar *en* to $Mg(BH_4)_2$, which displays an asymmetric mixing of Mg^{2+} with one *en* and two BH_4^-. Yan et al. [41] systematically investigated the influence of NH_3, where the crystal structure and the ionic conduction properties depend on the number of NH_3 in $Mg(BH_4)_2\cdot nNH_3$. Fig. 7(c) shows the crystal structure of $Mg(BH_4)_2\cdot NH_3$, which builts by zig-zag chains of -BH_4-Mg-BH_4-Mg- along the *b*-axis revealing a high degree of flexibility [41]. The ionic conductivity of $Mg(BH_4)_2\cdot NH_3$ was reported to be 3.3×10^{-4} S cm^{-1} at 80 °C. Changing the number of NH_3 to noninteger values such as 1.6, the ionic conductivity could be further improved, e.g., to 3.5×10^{-4} S cm^{-1} at 50 °C for $Mg(BH_4)_2\cdot 1.6NH_3$ [46]. Notice, that this is in fact a composite consisting of two crystalline compounds, $0.4Mg(BH_4)_2\cdot NH_3$-$0.6Mg(BH_4)_2\cdot 2NH_3$. By combining with metal oxide nanopowders [46,154] (such as MgO, Al_2O_3), $Mg(BH_4)_2\cdot 1.6NH_3$ could be converted to more conductive amorphous state with conductivities improved up to ~10^{-5} S cm^{-1} at room temperature and ~10^{-3} S cm^{-1} at 70 °C (Fig. 7(d)). More recently, Wang et al. [155] reported the observation of Mg^{2+} conductivity of 10^{-4} S cm^{-1} at room temperature in $Mg(BH_4)_2\cdot 1.5NH_3$, after cooperation with the oxygen vacancies on the surface of metal oxide nanopowders. They discovered that Mg^{2+} conductivity is enhanced by surface oxygen vacancy of the metal oxide nanopowders introduced to $Mg(BH_4)_2\cdot 1.5NH_3$. Fig. 7(e) demonstrated that the $Mg(BH_4)_2\cdot 1.5NH_3$-60 wt.% YSZ nanocomposite allows the stable Mg^{2+} stripping/plating for 300 cycles. So far, a big progress has been made in the $Mg(BH_4)_2$-based solid-state electrolytes. However, the electrochemical stabilities of magnesium borohydride based materials are generally limited to 1.2 V *vs.* Mg/Mg^{2+}, which is only compatible with low voltage cathode materials such as titanium sulphides. A new magnesium borohydride based electrolyte was recently developed using tetrahydrofurane, $O(CH_2)_4$, as ligand. The material was stabilized using magnesium oxide nano-particles to form a composite, $Mg(BH_4)_2\cdot 1.5THF$-MgO(75 wt.%), displayed high Mg^{2+} conductivity, $\sigma(Mg^{2+})$ ~10^{-4} S cm^{-1} at 70 °C, a high cationic transport number of $t_{ion} = 0.99$, and cyclic voltammetry revealed an oxidative stability of ~1.2 V *vs.* Mg/Mg^{2+}. This electrolyte is stable towards magnesium electrodes and allows construction of a proof-of-concept rechargeable solid-state magnesium battery with a magnesium metal anode and a TiS_2 cathode, i.e. $Mg|Mg(BH_4)_2\cdot 1.5THF$-MgO(75 wt.%)$|Mg_yTiS_2$ [47]. A maximum discharge capacity of 94.2 $mAhg^{-1}$ was displayed, which corresponds to $y = 0.2$ in Mg_yTiS_2. Therefore, the cationic conductivity may be further improved by the design of new types of composite materials and more efforts are required to be taken to improve the electrochemical stability, e.g. by surface coating of electrolytes.

6. Conclusions and perspectives

In this work, we summarize the physical and chemical properties of $Mg(BH_4)_2$ with its potential applications in hydrogen storage, physisorption and batteries. Especially, we put the emphasis

on the recent progress of the latter two research directions, which are not well discussed in the previous reviews. $Mg(BH_4)_2$, as a typical high capacity hydrogen storage material, suffers from the formation of the stable intermediate $[B_{12}H_{12}]^{2-}$, the strong B-B bonding of which makes the rehydrogenation condition very harsh. In contrast, lower borane intermediate $[B_3H_8]^{2-}$ facilitates rehydrogenation even at a mild condition of 100 °C. These results suggest that how to control the formation of lower borane intermediate with weak B-B bonding during the dehydrogenation process is a crucible for the improvement of reversible hydrogen storage in $Mg(BH_4)_2$. γ-$Mg(BH_4)_2$ is the first and only example of solid hydrides which owns a unique hydridic porous framework exhibiting interesting gas physisorption behavior. A diffraction-based methodology was developed to investigate adsorption properties for several gases (N_2, C_2H_6, Kr, Xe) from both macro- and microscopic points of view. The difference of the hydridic porous framework with that of the metal organic framework on the gas adsorption behavior is expected to be clarified, which may help develop new porous materials with superior gas adsorption. $Mg(BH_4)_2$ also shows ion conductivity in THF or DME, leading to the potential application in battery systems. Weakening the coordination between Mg^{2+} and $[BH_4]^-$ by replacing $[BH_4]^-$ to other anions such as AlH_4^-, NH_2^-, or introducing neutral molecules $NH_2(CH_2)_2NH_2$, NH_3 and NH_3BH_3 is an important approach to improve the ionic conductivity of $Mg(BH_4)_2$-based materials for solid-state electrolytes. Extensive efforts are expected to be put on finding effective solutions to further improve the ionic conductivity that satisfies the practical applications of Mg rechargeable batteries. In addition, experimental investigations are expected to combine with advanced calculation technology and cutting edge *in-situ*/operando analysis technology in the future, in order to elucidate the mechanism of each function and provide insightful information for further improvement of the relevant functions. Thus, obtained achievement will not only help develop $Mg(BH_4)_2$ for energy related applications, but also give important knowledge for the deeper understanding of other hydrides and the discovery of novel functions as well.

Acknowledgments

This work was financially supported by the National Natural Science Foundation of China Projects (Nos. 52171205, 21975168 and 52101249), the Anhui Provincial Natural Science Foundation for Excellent Youth Scholars (No. 2108085Y16), the Youth Science and Technology Fund Project of China Machinery Industry Group Co., Ltd. (No. QNJJ-ZD-2022-01) and the Natural Science Foundation of Anhui Province (No. 2108085QE191). This work was also supported by the Independent Research Fund Denmark for Technology and Production (No. 9041-00226B), by FNRS (PDR T.0169.13, EQP U.N038.13, J.0164.17, CdR J.0073.20) and the Communauté Française de Belgique under Grant ARC 18/23-093.

References

[1] S.S. Kumar, H. Lim, Energy Rep. 8 (2022) 13793–13813.
[2] R.D. McCarty, Selected Properties of Hydrogen (Engineering Design Data), US Department of Commerce, National Bureau of Standards, 1981.
[3] S.A. Sherif, D.Y. Goswami, E.K.L. Stefanakos, A. Steinfeld, Handbook of Hydrogen Energy, CRC Press, Boca Raton, Florida, 2014.
[4] K. Sasaki, H.W. Li, A. Hayashi, J. Yamabe, T. Ogura, S.M. Lyth, Hydrogen Energy Engineering, Springer, Tokyo, 2016.
[5] Q. Li, X. Peng, F. Pan, J. Magnes. Alloy. 9 (2021) 2223–2224.
[6] Q. Li, X. Lin, Q. Luo, Y. Chen, J. Wang, B. Jiang, F. Pan, Int. J. Miner. Metall. Mater. 29 (2022) 32–48.
[7] F. Marques, M. Balcerzak, F. Winkelmann, G. Zepon, M. Felderhoff, Energy Environ. Sci. 14 (2021) 5191–5227.
[8] G. Liang, J. Huot, S. Boily, A. Van Neste, R. Schulz, J. Alloy. Compd. 292 (1999) 247–252.
[9] H. Leng, Y. Pan, Q. Li, K.C. Chou, Int. J. Hydrog. Energy 39 (2014) 13622–13627.
[10] S. Orimo, Y. Nakamori, J.R. Eliseo, A. Zu, C.M. Jensen, Chem. Rev. 107 (2007) 4111–4132.
[11] M.B. Ley, L.H. Jepsen, Y. Lee, Y.W. Cho, M.B. Von Colbe, M. Dornheim, M. Rokni, J.O. Jensen, M. Sloth, Y. Filinchuk, J.E. Jørgensen, F. Besenbacher, T.R. Jensen, Mater. Today 17 (2014) 122–128.
[12] B. Bogdanović, M. Felderhoff, A. Pommerin, F. Schüth, N. Spielkamp, Adv. Mater. 18 (2006) 1198–1201.
[13] M. Paskevicius, L.H. Jepsen, P. Schouwink, R. Černý, D.B. Ravnsbæk, Y. Filinchuk, M. Dornheim, F. Besenbacher, T.R. Jensen, Chem. Soc. Rev. 46 (2017) 1565–1634.
[14] K. Wang, Z. Pan, X. Yu, J. Alloy. Compd. 794 (2019) 303–324.
[15] R. Singh, Int. J. Hydrog. Energy 47 (2022) 26549–26573.
[16] J.B. Grinderslev, M.B. Amdisen, L.N. Skov, K.T. Møller, L.G. Kristensen, M. Polanski, M. Heere, T.R. Jensen, J. Alloy. Compd. 896 (2022) 163014.
[17] K. Suárez-Alcántara, J.R.T. García, Materials 14 (2021) 2561.
[18] E.M. Dematteis, M.B. Amdisen, T. Autrey, J. Barale, M.E. Bowden, C.E. Buckley, Y.W. Cho, S. Deledda, M. Dornheim, P. De Jongh, J.B. Grinderslev, G. Gizer, V. Gulino, B.C. Hauback, M. Heere, T.W. Heo, T.D. Humphries, T.R. Jensen, S.Y. Kang, Y.S. Lee, H.W. Li, S. Li, K.T. Møller, P. Ngene, S.I. Orimo, M. Paskevicius, M. Polanski, S. Takagi, L. Wan, B.C. Wood, M. Hirscher, M. Baricco, Prog. Energy 4 (2022) 032009.
[19] A. Schneemann, J.L. White, S. Kang, S. Jeong, L.F. Wan, E.S. Cho, T.W. Heo, D. Prendergast, J.J. Urban, B.C. Wood, M.D. Allendorf, V. Stavila, Chem. Rev. 118 (2018) 10775–10839.
[20] E. Hadjixenophontos, E.M. Dematteis, N. Berti, A.R. Wołczyk, P. Huen, M. Brighi, T.T. Le, A. Santoru, S. Payandeh, F. Peru, A.H. Dao, Y. Liu, M. Heere, Inorganics 8 (2020) 17.
[21] Y. Ma, T. Zhang, W. He, Q. Luo, Z. Li, W. Zhang, J. He, Q. Li, Int. J. Hydrog. Energy 45 (2020) 12048–12070.
[22] Y. Lv, Y. Wu, Prog. Nat. Sci. Mater. Int. 31 (2021) 809–820.
[23] O. Zavorotynska, A. El-Kharbachi, S. Deledda, B.C. Hauback, Int. J. Hydrog. Energy 41 (2016) 14387–14403.
[24] Y. Filinchuk, R. Černý, H. Hagemann, Chem. Mater. 21 (2009) 925–933.
[25] J.H. Her, P.W. Stephens, Y. Gao, G.L. Soloveichik, J. Rijssenbeek, M. Andrus, J.C. Zhao, Acta Crystallogr. Sect. B-Struct. Sci. 63 (2007) 561–568.
[26] Y. Filinchuk, B. Richter, T.R. Jensen, V. Dmitriev, D. Chernyshov, H. Hagemann, Angew. Chem. Int. Ed. 50 (2011) 11162–11166.
[27] B. Richter, D.B. Ravnsbæk, N. Tumanov, Y. Filinchuk, T.R. Jensen, Dalton Trans. 44 (2015) 3988–3996.
[28] V. Ban, A.V. Soloninin, A.V. Skripov, J. Hadermann, A. Abakumov, Y. Filinchuk, J. Phys. Chem. C 118 (2014) 23402–23408.
[29] https://www.energy.gov/eere/fuelcells/doe-technical-targets-onboard-hydrogen-storage-light-duty-vehicles 2022.
[30] E. Wiberg, R. Bauer, Z. Für Naturforsch. B 5 (1950) 397–398.
[31] V.N. Konoplev, M. Bakulina, Russ. Chem. Bull. 20 (1971) 136–138.
[32] K.N. Semenenko, S.P. Shilkin, V.B. Polyakova, Russ. Chem. Bull. 24 (1975) 661–663.
[33] K. Chłopek, C. Frommen, A. Léon, O. Zabara, M. Fichtner, J. Mater. Chem. 17 (2007) 3496–3503.
[34] H.W. Li, K. Kikuchi, Y. Nakamori, K. Miwa, S. Towata, S. Orimo, Scr. Mater. 57 (2007) 679–682.
[35] T. Matsunaga, F. Buchter, K. Miwa, S. Towata, S. Orimo, A. Züttel, Renew. Energy 33 (2008) 193–196.
[36] H.W. Li, K. Kikuchi, Y. Nakamori, N. Ohba, K. Miwa, S. Towata, S. Orimo, Acta Mater. 56 (2008) 1342–1347.
[37] R.J. Newhouse, V. Stavila, S.J. Hwang, L.E. Klebanoff, J.Z. Zhang, J. Phys. Chem. C 114 (2010) 5224–5232.
[38] G.L. Soloveichik, Y. Gao, J. Rijssenbeek, M. Andrus, S. Kniajanski, R.C. Bowman, S.J. Hwang, J.C. Zhao, Int. J. Hydrog. Energy 34 (2009) 916–928.
[39] R. Mohtadi, M. Matsui, T.S. Arthur, S.J. Hwang, Angew. Chem. 124 (2012) 9918–9921.
[40] E. Roedern, R.S. Kühnel, A. Remhof, C. Battaglia, Sci. Rep. 7 (2017) 46189.
[41] Y. Yan, W. Dononelli, M. Jørgensen, J.B. Grinderslev, Y.S. Lee, Y.W. Cho, R. Černý, B. Hammer, T.R. Jensen, Phys. Chem. Chem. Phys. 22 (2020) 9204–9209.
[42] K. Kisu, S. Kim, M. Inukai, H. Oguchi, S. Takagi, S. Orimo, ACS Appl. Energy Mater. 3 (2020) 3174–3179.
[43] M. Heere, A.L. Hansen, S.H. Payandeh, N. Aslan, G. Gizer, M.H. Sørby, B.C. Hauback, C. Pistidda, M. Dornheim, W. Lohstroh, Sci. Rep. 10 (2020) 1–11.
[44] E. Roedern, R.S. Kühnel, A. Remhof, C. Battaglia, Sci. Rep. 7 (2017) 1–6.
[45] R.Le Ruyet, R. Berthelot, E. Salager, P. Florian, B. Fleutot, R. Janot, J. Phys. Chem. C 123 (2019) 10756–10763.
[46] Y. Yan, J.B. Grinderslev, M. Jørgensen, L.N. Skov, J. Skibsted, T.R. Jensen, ACS Appl. Energy Mater. 3 (2020) 9264–9270.
[47] L.N. Skov, J.B. Grinderslev, A. Rosenkranz, Y.S. Lee, T.R. Jensen, Batter. Supercaps 5 (2022) e202200163.
[48] M.A.N. Ahmad, N. Sazelee, N.A. Ali, M. Ismail, Energies 15 (2022) 862.
[49] I. Dovgaliuk, I. Senkovska, X. Li, V. Dyadkin, Y. Filinchuk, D. Chernyshov, Angew. Chem. Int. Ed. 60 (2021) 5250–5256.
[50] I.H. Nayyar, B. Ginovska, M. Bowden, G. Edvenson, B. Tran, T. Autrey, J. Phys. Chem. A 126 (2022) 444–452.
[51] Z. Ma, D.R. MacFarlane, M. Kar, Batter. Supercaps 2 (2019) 115–127.
[52] J. Kollonitsch, O. Fuchs, V. Gábor, Nature 173 (1954) 125–126.
[53] H.C. Brown, E.J. Mead, B.C.S. Rao, J. Am. Chem. Soc. 77 (1955) 6209–6213.
[54] R. Koster, Angew. Chem. 69 (1957) 94.

[55] J. Plešek, S. Heřmánek, Collect. Czechoslov. Chem. Commun. 31 (1966) 3845–3858.
[56] Y.S. Au, Y. Yan, K.P. de Jong, A. Remhof, P.E. de Jongh, J. Phys. Chem. C 118 (2014) 20832–20839.
[57] V.N. Konoplev, Synthesis of magnesium borohydride, Zhurnal Neorg. Khimii. 25 (1980) 1737–1740.
[58] A. Bateni, S. Scherpe, S. Acar, M. Somer, Energy Procedia 29 (2012) 26–33.
[59] P. Zanella, L. Crociani, N. Masciocchi, G. Giunchi, S. Uniti, V. Pado, S. Chimiche, V. Uni, V. Valleggio, E. Spa, Inorg. Chem. 46 (2007) 9039–9041.
[60] Z.G. Zhang, S.F. Zhang, H. Wang, J.W. Liu, M. Zhu, J. Alloy. Compd. 505 (2010) 717–721.
[61] R.A. Varin, C. Chiu, Z.S. Wronski, J. Alloy. Compd. 462 (2008) 201–208.
[62] G. Severa, E. Rönnebro, C.M. Jensen, Chem. Commun. 46 (2010) 421–423.
[63] C. Pistidda, S. Garroni, F. Dolci, E.G. Bardají, A. Khandelwal, P. Nolis, M. Dornheim, R. Gosalawit, T. Jensen, Y. Cerenius, S. Suriñach, M.D. Baró, W. Lohstroh, M. Fichtner, J. Alloy. Compd. 508 (2010) 212–215.
[64] H.W. Li, T. Matsunaga, Y. Yan, H. Maekawa, M. Ishikiriyama, S. Orimo, J. Alloy. Compd. 505 (2010) 654–656.
[65] M.P. Pitt, C.J. Webb, M. Paskevicius, D. Sheptyakov, C.E. Buckley, E.M. Gray, J. Phys. Chem. C 115 (2011) 22669–22679.
[66] S. Gupta, I.Z. Hlova, T. Kobayashi, R.V. Denys, F. Chen, I.Y. Zavaliy, M. Pruski, V.K. Pecharsky, Chem. Commun. 49 (2013) 828–830.
[67] N.A. Strange, N. Leick, R.T. Bell, M.A. Fitzgerald, S. Pylypenko, A. Schneemann, V. Stavila, T. Gennett, Chem. Mater. 34 (2022) 10940–10951.
[68] R. Černý, N. Penin, H. Hagemann, Y. Filinchuk, J. Phys. Chem. C 113 (2009) 9003–9007.
[69] M.D. Riktor, M.H. Sørby, K. Chłopek, M. Fichtner, F. Buchter, A. Züttel, B.C. Hauback, J. Mater. Chem. 17 (2007) 4939–4942.
[70] W.I.F. David, S.K. Callear, M.O. Jones, P.C. Aeberhard, S.D. Culligan, A.H. Pohl, S.R. Johnson, K.R. Ryan, J.E. Parker, P.P. Edwards, C.J. Nuttall, A. Amieiro-Fonseca, Phys. Chem. Chem. Phys. 14 (2012) 11800–11807.
[71] M. Paskevicius, M.P. Pitt, C.J. Webb, D.A. Sheppard, U. Filsø, E.M. Gray, C.E. Buckley, J. Phys. Chem. C 116 (2012) 15231–15240.
[72] O. Zavorotynska, S. Deledda, J.G. Vitillo, I. Saldan, M.N. Guzik, M. Baricco, J.C. Walmsley, J. Muller, B.C. Hauback, Energies 8 (2015) 9173–9190.
[73] S. Guo, H.Y.L. Chan, D. Reed, D. Book, J. Alloy. Compd. 580 (2013) S296–S300.
[74] O. Friedrichs, A. Remhof, A. Borgschulte, F. Buchter, S.I. Orimo, A. Züttel, Phys. Chem. Chem. Phys. 12 (2010) 10919–10922.
[75] M. Dimitrievska, J.L. White, W. Zhou, V. Stavila, L.E. Klebanoffc, T.J. Udovicb, L.E. Klebanoff, T.J. Udovic, Phys. Chem. Chem. Phys. 18 (2016) 25546–25552.
[76] L.F. Wan, T. Autrey, B.C. Wood, J. Phys. Chem. Lett. 13 (2022) 1908–1913.
[77] J. Voss, J.S. Hummelshøj, Z. Łodziana, T. Vegge, J. Phys. Condens. Matter. 21 (2008) 12203.
[78] B.L. Tran, T.N. Allen, M.E. Bowden, T. Autrey, C.M. Jensen, Inorganics 9 (2021) 41.
[79] R.T. Bell, N.A. Strange, N. Leick, V. Stavila, M.E. Bowden, T.S. Autrey, T. Gennett, ACS Appl. Energy Mater. 4 (2021) 1704–1713.
[80] J. Zheng, H. Cheng, X. Xiao, M. Chen, L. Chen, Int. J. Hydrog. Energy 44 (2019) 24292–24300.
[81] I. Saldan, Int. J. Hydrog. Energy 41 (2016) 11201–11224.
[82] Y. Zhang, E. Majzoub, V. Ozoliņš, C. Wolverton, J. Phys. Chem. C 116 (2012) 10522–10528.
[83] J.K. Olson, A.I. Boldyrev, Comput. Theor. Chem. 967 (2011) 1–4.
[84] R. Moury, A. Gigante, A. Remhof, E. Roedern, H. Hagemann, Dalton Trans. 49 (2020) 12168–12173.
[85] S.-J. Hwang, R.C. Bowman, J.W. Reiter, G.L.S. Rijssenbeek, J.C. Zhao, H. Kabbour, C.C. Ahn, J. Phys. Chem. C. 112 (2008) 3164–3169.
[86] Y. Yan, H.W. Li, H. Maekawa, M. Aoki, T. Noritake, M. Matsumoto, K. Miwa, S. Towata, S. Orimo, Mater. Trans. 52 (2011) 1443–1446.
[87] H.W. Li, K. Miwa, N. Ohba, T. Fujita, T. Sato, Y. Yan, S. Towata, M.W. Chen, S. Orimo, Nanotechnology 20 (2009) 204013.
[88] R. Černý, Y. Filinchuk, H. Hagemann, K. Yvon, Angew. Chem. Int. Ed. 46 (2007) 5765–5767.
[89] I. Saldan, C. Frommen, I. Llamas-Jansa, G.N. Kalantzopoulos, S. Hino, B. Arstad, R.H. Heyn, O. Zavorotynska, S. Deledda, M.H. Sørby, H. Fjellvåg, B.C. Hauback, Int. J. Hydrog. Energy 40 (2015) 12286–12293.
[90] M. Chong, A. Karkamkar, T. Autrey, S. Orimo, S. Jalisatgi, C.M. Jensen, Chem. Comm. 47 (2011) 1330–1332.
[91] A. Gigante, N. Leick, A.S. Lipton, B. Tran, N.A. Strange, M. Bowden, M.B. Martinez, R. Moury, T. Gennett, H. Hagemann, T.S. Autrey, ACS Appl. Energy Mater. 4 (2021) 3737–3747.
[92] H.W. Li, E. Akiba, S.I. Orimo, J. Alloy. Compd. 580 (2013) S292–S295.
[93] J.L. White, R.J. Newhouse, J.Z. Zhang, T.J. Udovic, V. Stavila, J. Phys. Chem. C 120 (2016) 25725–25731.
[94] H.W. Li, Y. Yan, S.I. Orimo, A. Züttel, C.M. Jensen, Energies 4 (2011) 185–214.
[95] Y. Nakamori, S. Orimo, Storage Mater. Chem. 4 (2008) 420–449.
[96] V. Ozolins, E.H. Majzoub, C. Wolverton, J. Am. Chem. Soc. 131 (2009) 230–237.
[97] J. Zheng, X. Xiao, L. Zhang, S. Li, H. Ge, L. Chen, J. Mater. Chem. A 5 (2017) 9723–9732.
[98] P. Schouwink, V. D'Anna, M.B. Ley, L.M. Lawson Daku, B. Richter, T.R. Jensen, H. Hagemann, R. Černý, J. Phys. Chem. C 116 (2012) 10829–10840.
[99] A.A. Ibikunle, A.J. Goudy, Int. J. Hydrog. Energy 37 (2012) 12420–12424.
[100] T. Durojaiye, A. Ibikunle, A.J. Goudy, Int. J. Hydrog. Energy 35 (2010) 10329–10333.
[101] M.B. Ley, E. Roedern, P.M.M. Thygesen, T.R. Jensen, Energies 8 (2015) 2701–2713.
[102] E.G. Bardají, Z. Zhao-Karger, N. Boucharat, A. Nale, M.J. Van Setten, W. Lohstroh, E. Rahm, M. Catti, M. Fichtner, J. Phys. Chem. C 115 (2011) 6095–6101.
[103] Z. Fang, X. Kang, P. Wang, H. Li, S. Orimo, J. Alloy. Compd. 491 (2010) L1–L4.
[104] E. Grube, S.R.H. Jensen, U.G. Nielsen, T.R. Jensen, J. Alloy. Compd. 770 (2019) 1155–1163.
[105] J. Zheng, X. Xiao, Y. He, M. Chen, M. Liu, S. Li, L. Chen, J. Alloy. Compd. 762 (2018) 548–554.
[106] Y. Yang, M. Gao, Y. Liu, J. Wang, J. Gu, H. Pan, Z. Guo, Int. J. Hydrog. Energy 37 (2012) 10733–10742.
[107] Y. Liu, Y. Yang, Y. Zhou, Y. Zhang, M. Gao, H. Pan, Int. J. Hydrog. Energy 37 (2012) 17137–17145.
[108] J. Zheng, H. Cheng, X. Wang, M. Chen, X. Xiao, L. Chen, ACS Appl. Energy Mater. 3 (2020) 3033–3041.
[109] Y. Li, Y. Liu, X. Zhang, D. Zhou, Y. Lu, M. Gao, H. Pan, J. Mater. Chem. A 4 (2016) 8366–8373.
[110] G. Soloveichik, J.H. Her, P.W. Stephens, Y. Gao, J. Rijssenbeek, M. Andrus, J.C. Zhao, Inorg. Chem. 47 (2008) 4290–4298.
[111] X.B. Yu, Y.H. Guo, D.L. Sun, Z.X. Yang, A. Ranjbar, Z.P. Guo, H.K. Liu, S.X. Dou, J. Phys. Chem. C 114 (2010) 4733–4737.
[112] T. He, H. Wu, J. Chen, W. Zhou, G. Wu, Z. Xiong, T. Zhang, P. Chen, Phys. Chem. Chem. Phys. 15 (2013) 10487–10493.
[113] N.A. Ali, N.A. Sazelee, M. Ismail, Int. J. Hydrog. Energy 46 (2021) 31674–31698.
[114] I. Saldan, S. Hino, T.D. Humphries, O. Zavorotynska, M. Chong, C.M. Jensen, S. Deledda, B.C. Hauback, J. Phys. Chem. C 118 (2014) 23376–23384.
[115] J. Jiang, J. Wei, H. Leng, Q. Li, K.-C. Chou, Int. J. Hydrog. Energy 38 (2013) 10919–10925.
[116] X. Wang, X. Xiao, J. Zheng, Z. Hang, W. Lin, Z. Yao, M. Zhang, L. Chen, Int. J. Hydrog. Energy 46 (2021) 23737–23747.
[117] O. Zavorotynska, I. Saldan, S. Hino, T.D. Humphries, S. Deledda, B.C. Hauback, J. Mater. Chem. A 3 (2015) 6592–6602.
[118] M. Heere, O. Zavorotynska, S. Deledda, M.H. Sørby, D. Book, T. Steriotis, B.C. Hauback, RSC Adv. 8 (2018) 27645–27653.
[119] J. Zheng, X. Wang, X. Xiao, H. Cheng, L. Zhang, L. Chen, Chem. Eng. J. 412 (2021) 128738.
[120] E.G. Bardají, N. Hanada, O. Zabara, M. Fichtner, Int. J. Hydrog. Energy 36 (2011) 12313–12318.
[121] Z. Zhang, D. Gao, J. Zheng, A. Xia, Q. Zhang, L. Wang, L. Zhang, Chem. Eng. J. 460 (2023) 141690.
[122] J. Yuan, J. Chen, H. Huang, Y. Lv, B. Liu, Z. Li, B. Zhang, W. Lv, Y. Wu, Prog. Nat. Sci. Mater. Int. 31 (2021) 521–526.
[123] S. Kumar, A. Singh, K. Nakajima, A. Jain, H. Miyaoka, T. Ichikawa, G.K. Dey, Y. Kojima, Int. J. Hydrog. Energy 42 (2017) 22342–22347.
[124] N.N. Sulaiman, M. Ismail, S.N. Timmiati, K.L. Lim, Int. J. Energy Res. 45 (2021) 2882–2898.
[125] N. Juahir, N.S. Mustafa, F.A. Halim Yap, M. Ismail, Int. J. Hydrog. Energy 40 (2015) 7628–7635.
[126] Y. Yan, Y.S. Au, D. Rentsch, A. Remhof, P.E. de Jongh, A. Züttel, J. Mater. Chem. A 1 (2013) 11177–11183.
[127] X. Feng, J. Yuan, Y. Lv, B. Liu, H. Huang, B. Zhang, Y. Yan, S. Han, Y. Wu, Int. J. Hydrog. Energy 45 (2020) 16654–16662.
[128] J. Yuan, H. Huang, Z. Jiang, Y. Lv, B. Liu, B. Zhang, Y. Yan, Y. Wu, ACS Appl. Nano Mater. 4 (2021) 1604–1612.
[129] L. Zhang, J. Zheng, L. Chen, X. Xiao, T. Qin, Y. Jiang, S. Li, H. Ge, Q. Wang, Int. J. Hydrog. Energy 40 (2015) 14163–14172.
[130] Z. Jiang, J. Yuan, H. Han, Y. Wu, J. Alloy. Compd. 743 (2018) 11–16.
[131] A. Nale, F. Pendolino, A. Maddalena, P. Colombo, Int. J. Hydrog. Energy 41 (2016) 11225–11231.
[132] Y. Yang, Y. Liu, Y. Li, X. Zhang, M. Gao, H. Pan, J. Mater. Chem. A 3 (2015) 11057–11065.
[133] M. Fichtner, Z. Zhao-Karger, J. Hu, A. Roth, P. Weidler, Nanotechnology 20 (2009) 204029.
[134] M. Rueda, Ó. Benito-Román, A. Girella, P. Cofrancesco, C. Milanese, J. Energy Storage 31 (2020) 101674.
[135] P. Javadian, T.R. Jensen, Int. J. Hydrog. Energy 39 (2014) 9871–9876.
[136] D. Clémençon, C. Davoisne, J.N. Chotard, R. Janot, Int. J. Hydrog. Energy 44 (2019) 4253–4262.
[137] M.A. Wahab, Y. (Alec) Jia, D. Yang, H. Zhao, X. Yao, J. Mater. Chem. A 1 (2013) 3471–3478.
[138] J. Zheng, Z. Yao, X. Xiao, X. Wang, J. He, M. Chen, H. Cheng, L. Zhang, L. Chen, Int. J. Hydrog. Energy 46 (2021) 852–864.
[139] Q. Lai, K.F. Aguey-Zinsou, Sustain. Energy Fuels 1 (2017) 1308–1319.
[140] A. Schneemann, L.F. Wan, A.S. Lipton, Y.S. Liu, J.L. Snider, A.A. Baker, J.D. Sugar, C.D. Spataru, J. Guo, T.S. Autrey, M. Jørgensen, T.R. Jensen, B.C. Wood, M.D. Allendorf, V. Stavila, ACS Nano 14 (2020) 10294–10304.
[141] X. Wang, X. Xiao, J. Zheng, X. Huang, M. Chen, L. Chen, Int. J. Hydrog. Energy 45 (2020) 2044–2053.
[142] O. Zavorotynska, S. Deledda, G. Li, M. Matsuo, S. Orimo, B.C. Hauback, Angew. Chem. Int. Ed. 54 (2015) 10592–10595.
[143] I. Dovgaliuk, F. Nouar, C. Serre, Y. Filinchuk, D. Chernyshov, Chem. A Eur. J 23 (2017) 17714–17720.
[144] I. Dovgaliuk, V. Dyadkin, M. Vander Donckt, Y. Filinchuk, D. Chernyshov, ACS Appl. Mater. Interfaces 12 (2020) 7710–7716.
[145] A. Gotzias, A. Sapalidis, E. Favvas, Int. J. Hydrog. Energy 46 (2021) 19778–19787.

[146] N.P. Stadie, E. Callini, B. Richter, T.R. Jensen, A. Borgschulte, A. Züttel, J. Am. Chem. Soc. 136 (2014) 8181–8184.
[147] F. Cuevas, M.B. Amdisen, M. Baricco, C.E. Buckley, Y.W. Cho, P. de Jongh, L.M. de Kort, J.B. Grinderslev, V. Gulino, B.C. Hauback, M. Heere, T. Humphries, T.R. Jensen, S. Kim, K. Kisu, Y.S. Lee, H.W. Li, R. Mohtadi, K.T. Møller, P. Ngene, D. Noréus, S. Orimo, M. Paskevicius, M. Polanski, S. Sartori, L.N. Skov, M.H. Sørby, B.C. Wood, V.A. Yartys, M. Zhu, M. Latroche, Prog. Energy 4 (2022) 32001.
[148] Y. Shao, T. Liu, G. Li, M. Gu, Z. Nie, M. Engelhard, J. Xiao, D. Lv, C. Wang, J.G. Zhang, J. Liu, Sci. Rep. 3 (2013) 4–10.
[149] O. Tutusaus, R. Mohtadi, T.S. Arthur, F. Mizuno, E.G. Nelson, Y.V. Sevryugina, Angew. Chem. Int. Ed. 54 (2015) 7900–7904.
[150] T. Ikeshoji, E. Tsuchida, S. Takagi, M. Matsuo, S.I. Orimo, RSC Adv. 4 (2014) 1366–1370.
[151] M. Matsuo, H. Oguchi, T. Sato, H. Takamura, E. Tsuchida, T. Ikeshoji, S.I. Orimo, J. Alloy. Compd. 580 (2013) S98–S101.
[152] S. Higashi, K. Miwa, M. Aoki, K. Takechi, Chem. Commun. 50 (2014) 1320–1322.
[153] R.Le Ruyet, B. Fleutot, R. Berthelot, Y. Benabed, G. Hautier, Y. Filinchuk, R. Janot, ACS Appl. Energy Mater. 3 (2020) 6093–6097.
[154] Y. Yan, J.B. Grinderslev, T. Burankova, S. Wei, J.P. Embs, J. Skibsted, T.R. Jensen, Phys. Chem. Lett. 13 (2022) 2211–2216.
[155] Q. Wang, H. Li, R. Zhang, Z. Liu, H. Deng, W. Cen, Y. Yan, Y. Chen, Energy Storage Mater. 51 (2022) 630–637.